Full Coherent Frequency Conversion between Two Propagating Microwave Modes

Baleegh Abdo, Katrina Sliwa, Flavius Schackert, Nicolas Bergeal, Michael Hatridge, Luigi Frunzio, A. Douglas Stone, and Michel Devoret

Phys. Rev. Lett. **110**, 173902 — Published 26 April 2013

DOI: 10.1103/PhysRevLett.110.173902

Full coherent frequency conversion between two microwave propagating modes

Baleegh Abdo,* Katrina Sliwa, Flavius Schackert, Nicolas Bergeal,†
Michael Hatridge, Luigi Frunzio, A. Douglas Stone, and Michel Devoret
Department of Applied Physics, Yale University, New Haven, CT 06520, USA.
(Dated: March 7, 2013)

We demonstrate full frequency conversion in the microwave domain using a Josephson three-wave mixing device pumped at the difference between the frequencies of its fundamental eigenmodes. By measuring the signal output as a function of the intensity and phase of the three input signal, idler and pump tones, we show that the device functions as a controllable three-wave beam-splitter/combiner for propagating microwave modes at the single-photon level, in accordance with theory. Losses at the full conversion point are found to be less than 10^{-2}. Potential applications of the device include quantum information transduction and realization of an ultra-sensitive interferometer with controllable feedback.

PACS numbers: 42.65.Ky, 42.25.Hz, 85.25.Cp, 42.79.Fm, 85.25.-j

A quantum information transducer capable of converting the frequency of a quantum signal without introducing noise is one of the desirable modules in quantum communication [1, 2]. With such a device, one could teleport quantum superpositions of ground and excited states of qubits from one system to another one with a different transition frequency, without loss of coherence. If a quantum signal can be routed through different frequency channels, optimization of quantum calculation and communication can be advantageously separated.

The simplest scheme for performing frequency conversion is pumping a dispersive medium with nonlinearity χ_2 at precisely the frequency difference between the input and output frequencies [3–10]. Such nonlinear process known as parametric frequency conversion holds the promise of converting the frequency in a unitary, therefore noiseless, manner, namely, without adding loss or dephasing to the processed signal [11]. In the optical domain, although the intrinsic conversion process can be unitary [12–15], technical issues such as filtering the converted signal from noise photons generated via Raman processes and residual pump photons can limit the practical end-to-end conversion efficiency. In the microwave domain, nonlinear elements used in mixers, such as Schottky diodes are by contrast intrinsically dissipative and inevitably lead to unacceptable conversion losses. This raises the question as to whether a unitary full conversion of an input signal can be realized practically.

Here, we show that such noiseless full conversion is possible in the microwave domain by operating a dissipationless three-wave mixing element known as the Josephson parametric converter (JPC) [16–18], in a regime of conversion without photon gain. The JPC performs frequency conversion from 8 to 15 GHz with losses below 0.05 dB at full conversion, as opposed to a typical loss of 6 dB in microwave mixers. We reveal the unitary nature of the JPC conversion by utilizing wave interference between the three incommensurate frequencies intervening the device. The coherence of the conversion process is thus verified without having to face the challenge of calibrating the transmission between different input and output lines of disparate frequencies.

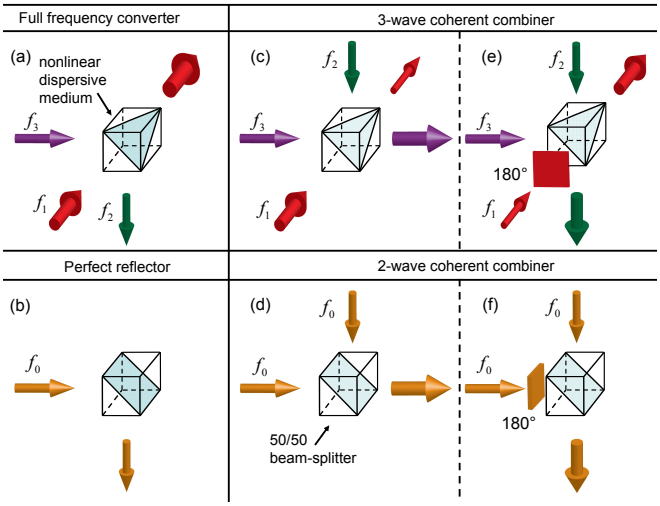

FIG. 1: (color online). In a 3-wave coherent converter, the scattered beams have different frequencies which we indicate using different colors: violet, green and red. Panel (a) depicts a nonlinear dispersive medium operated as a full frequency converter for the incident violet and green beams. Panel (b) depicts a splitter modified into a perfect mirror which constitutes the 2-wave analogue of the full frequency converter. Panels (c) and (e) introduce the relationship between frequency conversion and 3-wave interference. By operating the device, shown in panel (a), as a 3-wave 50/50 beam-combiner, one can coherently interfere two equal photon flux beams (green and violet) with disparate frequencies via frequency conversion through the third beam (red). Conversely, in a 2-wave coherent beam-splitter/combiner, complete interference can take place (panels (d) and (f)) when two equal intensity beams with the same frequency are incident at the beam-splitter.

To introduce the requirements obeyed by the properties of unitary frequency conversion, we compare, in Fig.

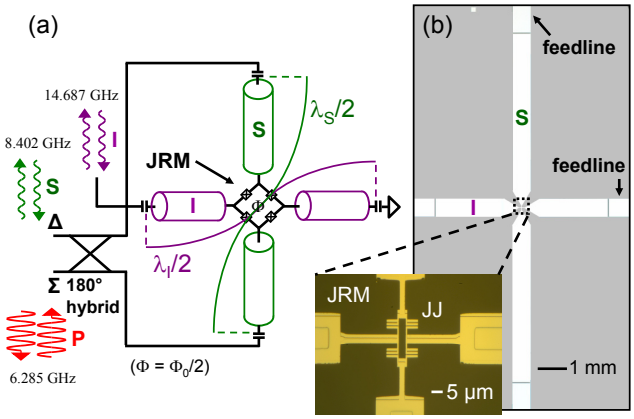

FIG. 2: (color online). Panel (a): circuit diagram of the JPC device. The JPC consists of two half-wave microstrip resonators denoted (S) and (I) which resonate at $f_S = 8.402\,\mathrm{GHz}$ and $f_I = 14.687\,\mathrm{GHz}$ with bandwidths of 95 MHz and 270 MHz respectively. The two resonators intersect at a Josephson ring modulator (JRM), which consists of four nominally identical Josephson junctions. The JRM is biased near half a flux quantum. Both S and I modes are excited differentially, while the pump (P) mode is commonly driven. Thus, S and P share the same spatial input ports and are fed through the difference (Δ) and sum (Σ) ports of a 180 degree hybrid. Panel (b): false color optical micrographs of the JPC device and the JRM.

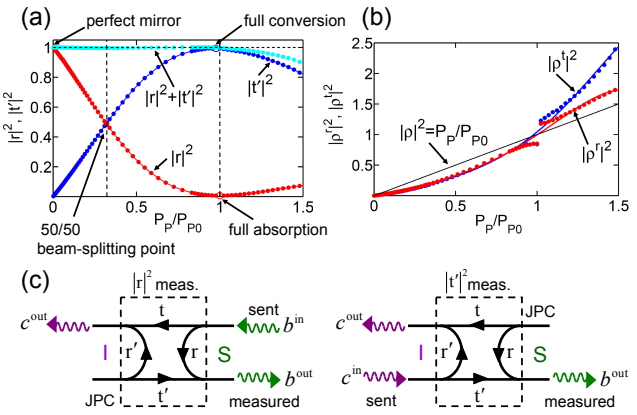

FIG. 3: (color online). (a) Reflection and conversion measurements of the JPC. The reflection (conversion) parameter $|r|^2$ ($|t'|^2$), drawn as filled red (blue) circles respectively, is measured at the signal port as a function of the normalized applied pump power. In the reflection (conversion) measurement a signal (idler) tone is applied at f_S (f_I) and the pump frequency is set to $f_P = f_I - f_S$. The cyan filled circles represent the sum $|r|^2 + |t'|^2$. The red and blue lines correspond to theory expressions (see supplementary material): $|t'|^2 = 4\left|\rho^t\right|^2/(1+\left|\rho^t\right|^2)^2$ and $|r|^2 = (1-|\rho^r|^2)^2/(1+|\rho^r|^2)^2$. Panel (b) plots using red (blue) circles the relation between the dimensionless parameter $|\rho^r|^2$ ($\left|\rho^t\right|^2$) employed in the fit of the reflection (conversion) data, and P_P/P_{P0}. The black line corresponds to the relation $|\rho|^2 = P_P/P_{P0}$. The red and blue curves are polynomial fits. (c) Signal flow graphs of the JPC in the conversion mode. In the reflection and conversion measurements shown on the left and the right, equal coherent beams are applied to the signal and idler ports, respectively.

1, a 3-wave coherent converter and a 2-wave coherent beam-splitter. Panel (a) depicts the desired case of unitary full frequency conversion of an incident propagating beam, i.e. a violet (high frequency) to a green (low frequency) beam, obtained by pumping a dispersive χ_2 medium with a red beam whose frequency is precisely the frequency difference. In panel (b) we depict the 2-wave analogue of such a device, that is the total reflector whose input and output beams have the same frequency and magnitude but propagate in different directions. Panels (c) and (e) depict the same 3-wave coherent converter shown in panel (a), now operated at the 50/50 beam-splitting point. At this working point, the device transmits half of the power of the input beams (green and violet) and converts the frequency of the other half using the third red (pump) beam. Hence, panel (c) and panel (e) describe destructive interference scenarios for the two equal photon flux input beams, resulting in the suppression of the output green and violet beams respectively. They also illustrate, (1) for a lossless destructive interference to take place between two frequencies, the power must be entirely converted to a third frequency, and (2) the output beams of such a device depend on the phases of all incident coherent beams. For further clarification of the role of the relative phases, we also show in panels (d) and (f) the 2-wave analogues of the destructive interference scenarios shown in panels (c) and (e).

Akin to the conceptual 3-wave converter depicted in Fig. 1, the JPC is a non-degenerate device with spatial and temporal separation between the idler and signal modes. Its input and output fields share however the same spatial port as shown in Fig. 2 (a) and must therefore be separated using a circulator. The idler and signal modes of the JPC are differential modes of the microstrip resonators of the device which intersect at a Josephson ring modulator (JRM) [17], as shown in Fig. 2 (b). The third mode supported by the device is a non-resonant common-mode drive (pump), whose frequency f_P is set to either the sum of the idler f_I and signal f_S frequencies or their difference. In the case where the pump frequency satisfies $f_P = f_I + f_S$, the device serves as a quantum-limited amplifier which can be used to readout the state of a solid state qubit in real time [19, 20]. In the present case where the pump frequency verifies $f_P = f_I - f_S$ ($f_I > f_S$), the device operates in frequency conversion mode with no photon gain. In this mode, as opposed to amplification [16], the device is not required, according to Caves theorem [21] to add any noise. Note that this working regime has been recently the subject of several

works in the areas of telecommunication and quantum information processing in optics [4–6, 22–24]. Also, in the recent work done at NIST [8, 9], the authors parametrically converted photons of different frequencies inside a microwave resonator coupled to a dc-SQUID. Phonon-photon parametric frequency conversion is also at play in the active cooling of a micro- or nano- mechanical resonator modes [1, 25, 26]. In our work, by contrast, it is photons from two different spatial and temporal modes that are interconverted.

When operated in conversion mode and under the stiff pump condition, the JPC can be described as an effective two-port beam-splitter whose scattering parameters can be adjusted by varying the pump tone of the device. In this mode, part of the incoming wave at the idler (signal) port is transmitted to the signal (idler) port after being downconverted (upconverted), via emission (absorption) of pump photons, while the remaining part is reflected off the idler (signal) port.

In Fig. 3 (a) we display measurements of the reflection parameter $|r|^2$ at the signal port (filled red circles) and the idler-to-signal conversion parameter $|t'|^2$ (filled blue circles) as a function of the normalized applied pump power P_P/P_{P0}, where P_{P0} is the pump power at which $|r|^2$ is minimum. In the reflection measurement, a coherent tone at $f_S = 8.402$ GHz is applied to the signal port with input power $P_{S0} = -123$ dBm, which corresponds to about 0.1 photons on average in the signal resonator, while in the conversion measurement an equivalent coherent tone at $f_I = 14.687$ GHz is applied to the idler port (as shown in panel (c)). The frequency of the applied pump tone is $f_P = 6.285$ GHz. Both measurements are taken using a spectrum analyzer centered at f_S in zero frequency span mode. The output power measured as a function of P_P/P_{P0} is normalized relative to the reflected signal power obtained with no applied pump power. There, the JPC has unity reflection, which can be measured within ± 0.5 dB accuracy due to a finite impedance mismatch in the output line.

As can be seen in Fig. 3, the splitting ratio between the converted and reflected portions of the beam is set by the device parameters and the pump amplitude. By varying the intensity of the pump, the splitting ratio of the device can be changed continuously from zero conversion and total reflection, to complete conversion and perfect absorption. It is important to mention that the input power applied to the idler port in the conversion measurement is set to yield, at the 50/50 beam-splitting working point, the same signal output power as the one measured in reflection for P_{S0}. It is remarkable that with this single calibration of input powers, which balances the output at the 50/50 beam-splitting point, the device satisfies quite well the equation of conservation of total photon number $|r|^2 + |t|^2 = 1$ ($|t| = |t'|$) in the range $P_P/P_{P0} < 1$ (see the cyan circles). When the

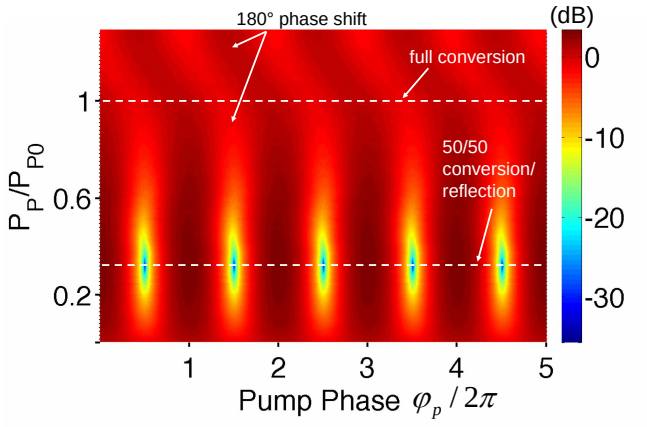

FIG. 4: (color online). Interference fringes of the reflected signal and the converted idler measured at the output of the signal port, at f_S, as a function of pump power and phase. The top (bottom) dashed line indicates the full conversion (50/50 beam-splitting) working point where the interference contrast is lowest (highest). For $P_P/P_{P0} > 1$ ($|\rho|^2 > 1$) a phase shift is observed in the interference pattern due to the change in the sign of the reflected signal amplitude, in accordance with theory (see supplementary material).

critical power is traversed $P_P/P_{P0} \gtrsim 1$, we observe a progressive breaking of unitarity $|r|^2 + |t'|^2 < 1$. This can be explained by increased nonlinear effects at elevated pump powers, resulting in frequency conversion to higher modes of the system. However, we find that in the vicinity of P_{P0}, the conversion loss, defined as the deviation of $|r|^2 + |t'|^2$ from unity, to be less than $\pm 10^{-2}$ within $\pm 2.5\%$ accuracy. We also observe a slight shift in power between the peak of the conversion and the minimum of the reflection data. The solid blue and red curves drawn using the equations shown in the legend of Fig. 3 (a), correspond to theory expressions to the conversion and reflection data respectively (see supplementary material). In panel (b) we plot, using filled red and blue circles, the dimensionless pump power parameters $|\rho^r|^2$ and $|\rho^t|^2$, which are used to fit the reflection and conversion data as a function of P_P/P_{P0}. The solid black line satisfying the relation $|\rho|^2 = P_P/P_{P0}$, corresponds to the expected dependence of $|\rho|^2$ on P_P/P_{P0} for the ideal JPC model with stiff pump approximation. The solid red and blue curves are polynomial fits to the $|\rho^r|^2$ and $|\rho^t|^2$ parameters. The fits satisfy three important properties: (1) they pass through the origin ($|\rho^{r,t}|^2 = 0$ for $P_P = 0$), (2) they have a leading linear term in the limit of small pump powers, (3) the fits for $|\rho^r|^2$ and $|\rho^t|^2$ coincide for $P_P/P_{P0} < 1$. They, therefore, show that the parameter $|\rho|^2$ is in fact a renormalized pump strength, at least for $P_P/P_{P0} < 1$.

In addition to the device dependence on pump power shown in Fig. 3, the relative pump phase plays an im-

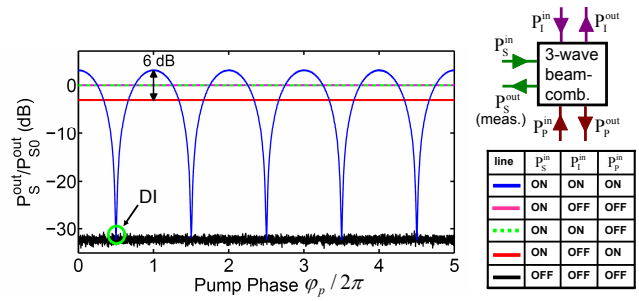

FIG. 5: (color online). The blue curve is a cross-section of the interference fringes shown in Fig. 4 at the 50/50 beam-splitting working point. The maximum and minimum points of the curve correspond to constructive and destructive interference (DI) conditions respectively. The other lines correspond to different reference measurements taken under the same experimental conditions as explained in the text. The input beams applied in each measurement are outlined in the table and the device cartoon on the right.

portant role as well. The downconverted idler and the upconverted signal acquire a phase shift which depends on the pump phase. We utilize this phase dependence as shown in Fig. 4 in order to sensitively interfere signal and idler beams. In this measurement, we applied two coherent tones to the signal and idler ports, having the same frequencies and powers as in the measurement of Fig. 3. We have also phase-locked the three independent coherent waves to the 10 MHz reference oscillator of a rubidium atomic clock. The color mesh in Fig. 4 depicts the interference fringes of the reflected and converted signals generated at the signal port as a function of P_P/P_{P0} and the relative pump phase. As can be seen in the figure, the interference contrast is low for $P_P \ll P_{P0}$ and $P_P/P_{P0} \to 1$ which correspond to almost total reflection and conversion respectively. A maximum interference contrast is obtained on the other hand for P_P/P_{P0} close to 0.32. We interpret this point as that where our device functions as a 50/50 beam-splitter/combiner. This is further shown in Fig. 5, where we display a cross-section of Fig. 4 at the point of maximum interference contrast. The wave interference modulation curve, shown in blue, is plotted as a function of the relative phase of the pump. The other lines represent different reference measurements taken under the same experimental conditions. The magenta line corresponds to the reflected signal power $P_{S0}^{\rm out}$ obtained without pump or idler tones and forms the reference level for the other measured powers. The dashed green line corresponds to the reflected signal power obtained with no pump but with an equivalent idler tone injected through the idler port. The fact that the dashed green line coincides with the magenta line shows that without pump the idler and signal modes are isolated. The red line represents the reflected signal power at the 50/50 beam-splitting working point and lies −3 dB below the reference (magenta) line as expected. Also, the relative power level of the peaks in the wave interference curve (blue), which correspond to constructive interference condition, lie as expected 6 dB (a factor of 4) above the red line obtained without idler. The black line corresponds to the noise floor measured without any signal. This noise is dominated by the high electron mobility transistor (HEMT) amplifier noise connected at the 4 K stage of our setup. Note that the minimum points of the wave interference curve (blue) correspond to destructive interference (DI) condition and coincide with the HEMT noise floor. By calculating the ratio of the average output power received in a destructive and constructive interference experiments (see supplementary material), we get a lower bound of −37.9 dB on the amount of destructive interference achieved by the device. This is equivalent to a coherent cancellation of 99.98% of input signal and idler beams.

Furthermore, in a separate interference measurement in which we varied the input power of the signal and idler beams (see supplementary material), we find that the device can handle a maximum input power of about −100 dBm, which corresponds to an average photon occupancy in the device of about 20 photons. Similar to Josephson amplifiers, this figure of merit can be improved by about one order of magnitude, by increasing the critical current of the junctions [17, 18]. We also note that the bandwidth of the present device (∼ 70 MHz) is limited by the bandwidths of the resonators. A wider bandwidth (∼ 500 MHz), could potentially be achieved by substituting the present JRM design with an inductively shunted ring [27].

In addition to quantum information transduction, the device has several potential useful applications, such as cooling of a readout cavity of a qubit by swapping the "hot" cavity photons, for instance at 8 GHz, by "cold" reservoir photons at 15 GHz, and realization of a Mach-Zehnder interferometer (MZI) scheme for microwaves with real-time feedback. In the latter scheme, the device would function as an interferometric 50/50 beam-combiner for incoming idler and signal waves. Assuming, for example, the information is carried by the phase of the signal in the MZI setup, while the idler serves as a reference, the information can be decoded from the incoming signal by measuring the generated interference at the signal port. Moreover, the setpoint of the device, which yields maximum phase sensitivity, can be maintained in-situ by compensating the shift using the pump phase.

Discussions with R. J. Schoelkopf and P. T. Rakich are gratefully acknowledged. The assistance of Michael Power in the fabrication process is highly appreciated. This research was supported by the NSF under grants DMR-1006060 and DMR-0653377; ECCS-1068642, the NSA through ARO Grant No. W911NF-09-1-0514,

IARPA under ARO Contract No. W911NF-09-1-0369, the Keck foundation, and Agence Nationale pour la Recherche under grant ANR07-CEXC-003. M.H.D. acknowledges partial support from College de France.

* Electronic address: baleegh.abdo@yale.edu
† Current address: LPEM-UMR8213/CNRS-ESPCI ParisTech-UPMC, 10 rue Vauquelin-75005 Paris, France.

[1] A. H. Safavi-Naeini and O. Painter, New J. Phys. **13**, 013017 (2011).
[2] C. A. Regal and K. W. Lehnert, J. Phys. Conf. Ser. **264**, 012025 (2011).
[3] J. Huang and P. Kumar, Phys. Rev. Lett. **68**, 2153 (1992).
[4] S. Zaske *et al.*, Phys. Rev. Lett. **109**, 147404 (2012).
[5] S. Ates *et al.*, Phys. Rev. Lett. **109**, 147405 (2012).
[6] M. T. Rakher, L. Ma, O. Slattery, X. Tang, and K. Srinivasan, Nature Photon. **4**, 786 (2010).
[7] S. Ramelow *et al.*, Phys. Rev. A **85**, 013845 (2012).
[8] E. Zakka-Bajjani *et al.*, Nature Phys. **7**, 599 (2011).
[9] F. Nguyen, E. Zakka-Bajjani, R. W. Simmonds, and J. Aumentado, Phys. Rev. Lett. **108**, 163602 (2012).
[10] L. G. Helt, M. Liscidini, and J. E. Sipe, J. Opt. Soc. Am. B **29**, 2199 (2012).
[11] J. Tucker and D. F. Walls, Ann. Phys. **52**, 1 (1969).
[12] M. A. Albota and F. N. C. Wong, Opt. Lett. **29**, 1449 (2004).
[13] A. P. Vandevender and P. G. Kwiat, J. Mod. Opt. **51**, 1433 (2004).
[14] C. Langrock *et al.*, Opt. Lett. **30**, 1725 (2005).
[15] J. S. Pelc, Q. Zhang, C. R. Phillips, L. Yu, Y. Yamamoto, and M. M. Fejer, Opt. Lett. **37**, 476 (2012).
[16] N. Bergeal *et al.*, Nature **465**, 64 (2010).
[17] B. Abdo *et al.*, Appl. Phys. Lett. **99**, 162506 (2011).
[18] B. Abdo, A. Kamal, M. H. Devoret, Phys. Rev. B **87**, 014508 (2013).
[19] R. Vijay, D. H. Slichter, and I. Siddiqi, Phys. Rev. Lett. **106**, 110502 (2011).
[20] M. Hatridge *et al.*, Science **339**, 178 (2013).
[21] C. M. Caves, Phys. Rev. D **26**, 1817-1839 (1982).
[22] S. Tanzilli *et al.*, Nature **437**, 116 (2005).
[23] M. G. Raymer, S. J. van Enk, C. J., McKinstrie, and H. J. McGuinness, Opt. Commun. **283**, 747 (2010).
[24] N. K. Langford *et al.*, Nature **478**, 360 (2011).
[25] J. D. Teufel *et al.*, Nature **475**, 359 (2011).
[26] R. Rivière *et al.*, Phy. Rev. A **83**, 063835 (2011).
[27] N. Roch *et al.*, Phys. Rev. Lett. **108**, 147701 (2012).